Active Compensation of the Deformation of a Magnetically Levitated Mover of a Planar Motor

C.H.H.M. Custers [1], I. Proimadis [2], J.W. Jansen [1,3], H. Butler [2,4], R. Tóth [2],
E.A. Lomonova [1], and P.M.J. van den Hof [2]
[1]Electromechanics and Power Electronics, Eindhoven University of Technology, 5600 MB Eindhoven, The Netherlands
[2]Control Systems, Eindhoven University of Technology, 5600 MB Eindhoven, The Netherlands
[3]Prodrive Technologies, Son, The Netherlands
[4]ASML, Veldhoven, The Netherlands

***Abstract*—The paper describes a commutation method used for the active compensation of the deformation of the magnetically levitated mover of a planar motor. The single-stage double layer planar motor under consideration comprises a stator with two coil arrays and a mover with permanent magnets, and is designed to perform positioning tasks with high accuracy. To minimize the deformation of the light-weight moving structure, which is exposed to a large force during actuation, its flexible behavior is considered in the commutation of the machine. The commutation decouples the rigid- and flexible-body modes and calculates the required currents in the coils to produce a desired force and torque, as well as the modal force to control the flexible modes deformation. To decouple the flexible modes in the commutation, the relation from coil current to deformation is required, which is obtained by the coupling of a mechanical model and electromagnetic model of the motor. Using a 25-axis laser interferometer system, the deformation of the mover is measured and the relation from coil current to modal deformation is experimentally validated. In a second experiment, the deformation reduction of the magnetically levitated translator is demonstrated.**

***Index Terms*—Electromagnetic devices, Position measurement**

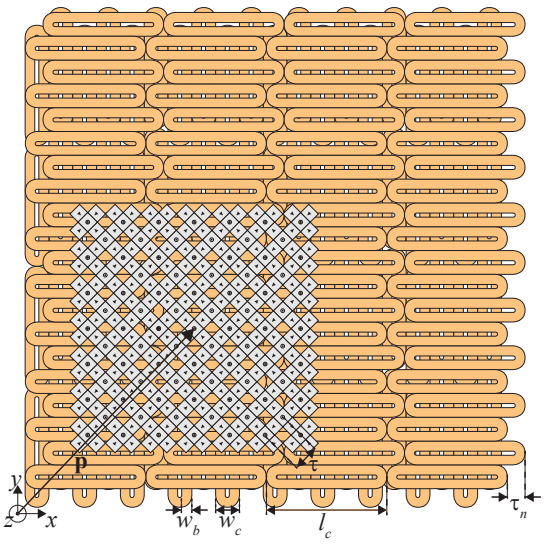

Fig. 1: Topology of the Double Layer Planar Motor [1], [5].

I. Introduction

In the semiconductor lithography industry, that produces billions of semiconductor circuits every year, the demands on actuation systems are ever increasing regarding accuracy and acceleration. The production process requires high-precision manufacturing while maintaining a high throughput rate. An essential part of the machines used for semiconductor lithography is the motion system which is responsible for positioning the wafer under a lens during exposure. The positioning devices used for this process usually consist of two actuation systems stacked on top of each other (dual-stage topology). One of the actuators performs a long-stroke motion in the XY-plane. The second short-stroke system, provides the nanometer accurate positioning of a wafer in 6 degrees-of-freedom. The long-stroke XY-positioning is often performed by a planar motor. In magnetically levitated planar motors [1]–[4], no bearings are present and stable levitation and propulsion of the moving body is achieved by means of magnetic fields. As a dual-stage topology typically leads to a heavy and bulky moving structure, which is disadvantageous in terms of power consumption and the amount of force that needs to be produced to reach high accelerations, alternatively, single-stage planar motors with a lightweight moving structure are subject of research [1], [5].

To achieve a high throughput rate with positioning systems, motion profiles with high acceleration are employed in the machines. These high accelerations result in extreme force on the motor parts, which in turn result in deformation of the mover and reduction of the positioning accuracy [6], [7]. Especially in devices where lightweight translators are used [1], [8] the deformations are significant as they have relatively low stiffness.

To control the flexible behavior of the aforementioned applications without increasing the stiffness by means of mechanical constructions, the principle of overactuation can be applied. Using additional actuators (or force inputs) than the minimum number needed to control the translation and the rotation of a magnetically levitated structure, the flexible modes of a system can be actively controlled. An example for rotating devices is

email: C.H.H.M.Custers@tue.nl

978-1-5386-9350-6/19/$31.00 ©2019 IEEE

given in [9], [10], where the rotor vibrations are attenuated. For 6 DoF systems, the principle of overactuation is described, among others, in [7], [11] where actuators at fixed locations are connected to the flexible body. The challenge of overactuation in magnetically levitated planar motors is the fact that there is no physical attachment of actuators to the moving flexible body. For moving-coil type of planar motors, however, the coils have a fixed distance with respect to the center of mass. As a result, the force is acting largely on the same location with respect to the center of mass of the translator, independent of the position. In moving-magnet planar motors, on the other hand, the force that is exerted by means of magnetic fields is spatially distributed over the flexible mover and, moreover, exhibits position-dependent effects, which imposes additional constraints on the overactuation approach. To overcome this challenge, an extended commutation algorithm is implemented in a motor with a magnetically levitated mover. The rigid body mode commutation algorithm decouples the developed force and torque and computes the required currents in the active coils, whereas the extended commutation algorithm additionally allows for control of the flexible body modes. This method of overactuation is analyzed and empirically demonstrated.

In this paper, the capabilities of a moving-magnet planar motor topology and its commutation algorithm towards over-actuation are investigated. The Double Layer Planar Motor (DLPM) [1], [5] is a bearing-less 6-DOF planar motor and has a lightweight translator with permanent magnets. The motor is designed as a single-stage alternative to existing dual-stage planar positioning devices. The stator consists of a double layer of coils, with in total 160 coils, of which maximum 40 can be active at a time. The paper is structured as follows: The design of the motor and the measurement system of the DLPM are discussed in Section II. In Section III, the commutation for the decoupling of rigid- and flexible-body modes is presented. The relation between an individual coil current and the excitation of a specific flexible mode is derived. This position dependent relation is incorporated in the commutation algorithm, thereby facilitating the active control of the flexible behavior of the translator. The obtained model is experimentally verified in Section IV, while in Section V the compensation of the flexible behavior is experimentally demonstrated.

II. The Double Layer Planar Motor

The Double Layer Planar Motor (DLPM) is designed to perform positioning tasks with high accuracy and has been optimized with respect to force production (in combination with minimal higher harmonic content) [12] and power losses.

A. Design

The electromagnetic configuration of the DLPM, consisting of coils and permanent magnets is depicted in Fig. 1. The translator consists of an aluminum carrier to which a total of 281 magnets are glued in a quasi-Halbach configuration to focus the magnetic field on the bottom side. Mirrors are placed on the top side of the mover to reflect the light of laser interferometers used for the position reconstruction. On the stator, a double layer of racetrack shaped coils produces the controllable magnetic field for stable levitation and propulsion of the translator. In each layer, 80 coils are present, which are designed in such a way that in both layers they produce an equal amount of lift force (z-direction) per unit of dissipated power. No iron is used, to prevent an attractive force between the stator and permanent magnet array. The coils of the bottom layer provide the force for propulsion in the x-direction. The top layer coils are oriented perpendicular to the bottom layer coils, and provide the propulsion force in the y-direction. To remove the heat produced by the coils, a cooling system is present on the stator. Properties of the of the DLPM are given in Table I. A picture of the manufactured DLPM prototype is shown in Fig. 2a.

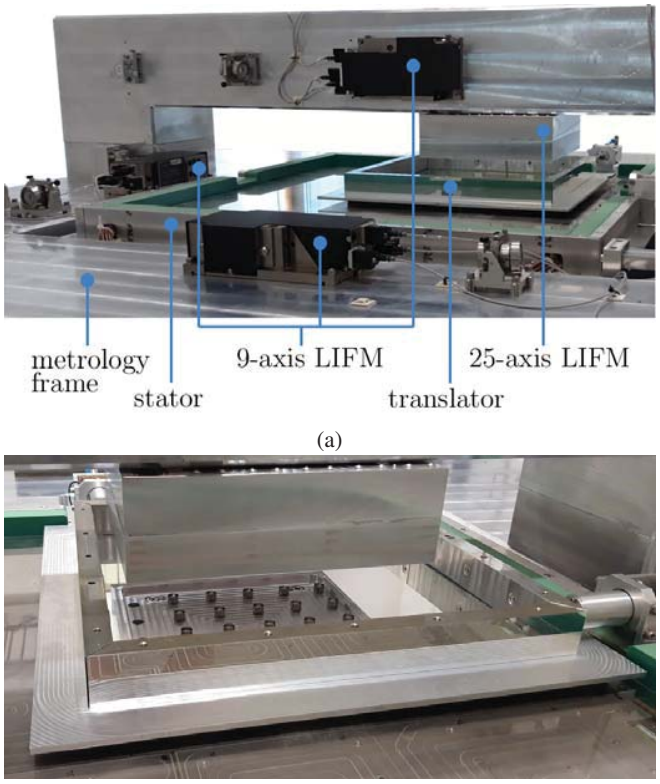

(a)

(b)

Fig. 2: Overview of the DLPM. a) The developed DLPM prototype with the various measurement systems. b) The 25-axis measurement system. The reflection of the laser interferometer heads on the top mirror of the translator can be partially seen.

The coils are powered by 40 power amplifiers, which means the maximum number of simultaneously active coils is equal to 40. To each amplifier, four coils, located in different quadrants of the stator, are connected through a multiplexer, which switches between the coils. A dSPACE 1006 (two quad-core processors) system with a sampling frequency of 8.3 kHz is used for real-time control and data acquisition.

TABLE I: Specifications of the DLPM.

	Parameter	Symbol	Value	Unit
Magnets	magnet pitch	τ	33.3	mm
	magnet pitch ($\tau/\sqrt{2}$)	τ_n	23.5	mm
	main magnet width	-	18.04	mm
	Halbach magnet width	-	15.04	mm
	magnet height	-	8.0	mm
	remanent flux density	-	1.28	T
	relative permeability	-	1.04	-
Top coils	coil length	l_c	156.0	mm
	coil width	w_c	30.0	mm
	bundle width	w_b	12.1	mm
	coil height	-	2.1	mm
Bottom coils	coil length	l_c	154.5	mm
	coil width	w_c	28.5	mm
	bundle width	w_b	11.4	mm
	coil height	-	7.8	mm

B. Measurement system

The position of the translator of the DLPM is reconstructed using the measurements from laser interferometer (LIFM) systems, which are shown in Fig. 2. To reject high-frequent disturbances affecting the stator due to floor vibrations or reaction forces during acceleration of the translator, the interferometer systems are placed on a metrology frame which is positioned around the stator and is supported by four air-mounts (Newport S-2000 Stabilizer). Two position measurement systems are considered for the experiments described in this paper.

Firstly, three 3-axis dual-pass laser interferometer systems (Agilent 10735A), which have a specified resolution of 0.16 nm, are used to reconstruct the relative 6 Degree-of-Freedom position of the translator with respect to the metrology frame. Each 3-axis device measures one of the displacement directions (x-, y- and z-direction) and two rotations. The position reconstructed by this system is used in the feedback control of the motor and based on the assumption that the translator is a rigid body.

Secondly, a 25-axis laser interferometer system (Attocube IDS3010), which has a specified resolution of 1 pm, is positioned above the translator. This measurement system is used to measure the flexible behavior of the translator. The laser interferometers are placed in a 5×5 grid with 40.0 mm $\times$ 40.0 mm spacing between the measurement points. The interferometer heads are placed in an aluminum block with the first eigenfrequency above 2 kHz, which is above the first four eigenfrequencies of the translator. The deformation of the translator can be measured by this system for a stroke of 80.0 mm in both the x- and y-directions. The data of the 25-axis LIFM system is read by a dSPACE DS1202 MicroLabBox, with a sampling frequency of 10 kHz.

III. Commutation

Commutation algorithms in planar motors are employed for feedback linearization and decoupling of the force and torque. In the DLPM, the so called direct wrench-current decoupling commutation is used [14], [15]. This algorithm has been developed for moving-magnet type planar motors to translate the desired force and torque of the motor to currents that are required in the coils to produce them. As the arms of the force producing coils towards the center of mass of the translator body are continuously varying in a moving-magnet planar motor, the direct wrench-current commutation is developed to actively control the force and torque components.

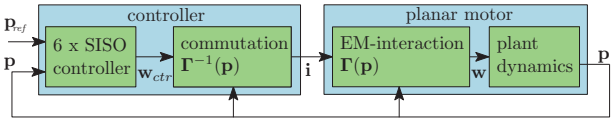

Fig. 3: Control scheme for rigid body mode control of the DLPM.

A. Rigid body mode commutation

The control scheme for rigid body mode control of the DLPM is shown in Fig. 3. The commutation algorithm calculates the coil currents in the active coils, which can be amplified independently. As the commutation decouples the force and torque components, each of the 6 DoFs is directly controlled by a SISO controller.

The direct wrench-current decoupling commutation algorithm is based on a magneto-static model, relating the current in a coil to the force and torque on the permanent magnets of the translator. Since the coil to magnet interaction in the DLPM can be described by the Lorentz force principle [12], the relation between the current in a coil and the force or torque on the translator is linear. The total force and torque components denoted by the wrench vector, $\mathbf{w}$, at a certain position, $\mathbf{p}$, can be obtained by the summation of all force and torque components produced by each of the individual coils. The wrench vector

$$\mathbf{w}(\mathbf{p}) = \left(\; F_x(\mathbf{p}) \; F_y(\mathbf{p}) \; F_z(\mathbf{p}) \; T_x(\mathbf{p}) \; T_y(\mathbf{p}) \; T_z(\mathbf{p}) \; \right)^\top , \quad (1)$$

is obtained through

$$\begin{aligned} \mathbf{w}(\mathbf{p}) &= \begin{pmatrix} {}^1k_{F_x}(\mathbf{p}) & {}^2k_{F_x}(\mathbf{p}) & \cdots & {}^{N_c}k_{F_x}(\mathbf{p}) \\ {}^1k_{F_y}(\mathbf{p}) & {}^2k_{F_y}(\mathbf{p}) & \cdots & {}^{N_c}k_{F_y}(\mathbf{p}) \\ {}^1k_{F_z}(\mathbf{p}) & {}^2k_{F_z}(\mathbf{p}) & \cdots & {}^{N_c}k_{F_z}(\mathbf{p}) \\ {}^1k_{T_x}(\mathbf{p}) & {}^2k_{T_x}(\mathbf{p}) & \cdots & {}^{N_c}k_{T_x}(\mathbf{p}) \\ {}^1k_{T_y}(\mathbf{p}) & {}^2k_{T_y}(\mathbf{p}) & \cdots & {}^{N_c}k_{T_y}(\mathbf{p}) \\ {}^1k_{T_z}(\mathbf{p}) & {}^2k_{T_z}(\mathbf{p}) & \cdots & {}^{N_c}k_{T_z}(\mathbf{p}) \end{pmatrix} \begin{pmatrix} {}^1i \\ {}^2i \\ \\ \vdots \\ {}^{N_c}i \end{pmatrix} \\ &= \mathbf{\Gamma}(\mathbf{p}) \; \mathbf{i}, \end{aligned} \quad (2)$$

where the commutation matrix, denoted by $\mathbf{\Gamma}(\mathbf{p})$, contains all coupling factors from a coil current to a certain wrench component. For example, ${}^1k_{F_x}(\mathbf{p})$ is the coupling factor from active coil 1 to the magnet array for the force in the x-direction at a certain position and orientation $\mathbf{p}$. This coupling factor represents in fact the relation from coil current to force produced in the x-direction for 1 A. In the same way the other coupling factors are defined for different coils and force or torque components. The number of active coils is denoted by N_c. In the DLPM, N_c is equal to 40. The position and orientation vector $\mathbf{p}$ is depicted in Fig. 1 and given by

$$\mathbf{p} = \left(\; p_x \quad p_y \quad p_z \quad \psi \quad \theta \quad \phi \; \right)^\top , \quad (3)$$

where ψ, θ and ϕ are the rotations around the x-, y- and z-axis, respectively. For real-time implementation purposes, the relation from coil current to force and torque components as a function of x and y is computed offline. By means of look-up tables, this data is available in the real-time control application, where the coupling factors in $\mathbf{\Gamma}$ are looked-up at each time instant.

To obtain the necessary currents $\mathbf{i}$ that will produce the desired wrench, the relation of (2) has to be inverted. The system of equations in (2) is under-determined, since multiple combinations of currents in the active coils can create the desired forces and torques. The minimum least squares norm solution [16] of (2) is given by

$$\mathbf{i} = \mathbf{\Gamma}^{\dagger}(\mathbf{p})\ \mathbf{w}, \tag{4}$$

where $\mathbf{\Gamma}^{\dagger}(\mathbf{p})$ is the Moore-Penrose pseudo inverse

$$\mathbf{\Gamma}^{\dagger}(\mathbf{p}) = \mathbf{\Gamma}^{\top}(\mathbf{p}) \left(\mathbf{\Gamma}(\mathbf{p})\ \mathbf{\Gamma}^{\top}(\mathbf{p})\right)^{-1}. \tag{5}$$

The coils closest to the center of the mover, based on the position of the mover in the x- and y-direction, are selected. Smooth switching of coils is ensured by applying a weighting function to the coil arrangement in both layers as described in [14], to prevent a sudden switch-off of current carrying coils.

Based on the error between the reference and the measured position, each rigid body mode is separately controlled by a single-input single-output (SISO) controller. The low-bandwidth controller, used for the experiments described in this paper, consists of a lead-lag filter and a roll-off low-pass filter. During the start-up phase of the machine, integral action is added to the controller to minimize the steady-state error. The bandwidth of the controllers is at 16 Hz, ensuring a position error less than 200 nm when the controllers have reached steady-state.

B. Commutation for overactuation

The matrix used for the rigid body mode commutation, which is described in (2), is extended by incorporation of the relation between a coil current and the flexible modes of the translator, to decouple these modes and provide possibilities for overactuation of the planar motor as described in [5], [17]. To this purpose, first, a mechanical model of the translator is developed.

1) Mechanical model: The flexible behavior of the translator of the DLPM, is described by discretization of a partial differential equation describing the mechanical dynamics. This results in a set of second-order differential equations. Such a model is usually described either in terms of nodal coordinates or modal coordinates [18], [19]. The nodal representation describes the motion dynamics of the selected points in the three-dimensional plane in terms of the associated mass ($\mathbf{M}$), spring ($\mathbf{K}$) and damping ($\mathbf{D}$) matrices,

$$\mathbf{M}\ddot{\mathbf{q}} + \mathbf{D}\dot{\mathbf{q}} + \mathbf{K}\mathbf{q} = \mathbf{f}, \tag{6}$$

where $\mathbf{q}$ and $\mathbf{f}$ are vectors describing the displacements and the forces, respectively, on the nodes in x, y and z direction, while the dots represent the derivative order, e.g. $\ddot{\mathbf{q}} = \frac{d^2\mathbf{q}}{dt^2}$.

TABLE II: Frequencies and damping coefficients of the first 4 flexible modes of the translator.

	Flexible mode number			
	1	2	3	4
Frequency [Hz]	226.5	546.5	698.5	1050
Damping coefficient [-]	0.011	0.027	0.010	0.015

The nodal model of a mechanical structure can be transformed into a modal description. In this way, the (usually) coupled differential equations in the nodal representation can be decoupled, thus allowing for a representation of the system which can be approximated by a reduced number of states. This transformation is achieved through a modal matrix $\mathbf{\Phi}$, which columns consist of the eigenvectors or modeshapes and is given by

$$\mathbf{\Phi} = \begin{pmatrix} \boldsymbol{\phi}_1 & \boldsymbol{\phi}_2 & \dots & \boldsymbol{\phi}_{N_{\text{flex}}} \end{pmatrix}, \tag{7}$$

where N_{flex} denotes the number of considered flexible modes. The relation between the nodal and the modal states is described by

$$\mathbf{q} = \mathbf{\Phi}\ \boldsymbol{\eta}, \tag{8}$$

where $\boldsymbol{\eta}$ are the so called modal states. Substituting (8) back to (6), left-multiplying it with the transposed modal matrix and normalizing the modal matrix with respect to the mass results in

$$\ddot{\boldsymbol{\eta}} + \mathbf{\Phi}^{\top}\mathbf{D}\mathbf{\Phi}\ \dot{\boldsymbol{\eta}} + \mathbf{\Phi}^{\top}\mathbf{K}\mathbf{\Phi}\ \boldsymbol{\eta} = \mathbf{\Phi}^{\top}\ \mathbf{f}, \tag{9}$$

where the input vector is the vector of forces. In (9), the derived modal stiffness matrices $\mathbf{\Phi}^{\top}\mathbf{K}\mathbf{\Phi}$ and $\mathbf{\Phi}^{\top}\mathbf{D}\mathbf{\Phi}$ are diagonal. These modal matrices are typically obtained from mechanical FEM software. The equation of motion in terms of modal coordinates of (9) can then be written as

$$\ddot{\boldsymbol{\eta}} + 2\mathbf{Z}\mathbf{\Omega}\ \dot{\boldsymbol{\eta}} + \mathbf{\Omega}^2\ \boldsymbol{\eta} = \mathbf{\Phi}^{\top}\ \mathbf{f}, \tag{10}$$

where $\mathbf{\Omega}$ is a diagonal matrix containing the natural frequencies [20], where each of these frequencies corresponds to a specific modeshape. The modal damping matrix $\mathbf{\Phi}^{\top}\mathbf{D}\mathbf{\Phi}$ is not necessarily diagonalized, therefore creating coupling between the modes. For this reason, a typical approach is to approximate it as a diagonal matrix $\mathbf{Z}$ with proportional damping coefficients ζ_n per mode, which can be tuned based on measurements of the mechanical system. To model the flexible mechanical behavior of the translator of the DLPM, the geometry of the translator is implemented in the mechanical FEM software ANSYS 17.1 [21], from which the modal matrix and eigenfrequencies are extracted. The eigenfrequencies and damping coefficients for the first four flexible modes, tuned using frequency response measurements are given in Table II. The first four modeshapes in the z-direction as a function of the x- and y-position are shown in Fig. 4. These modeshapes are typical for a free square plate.

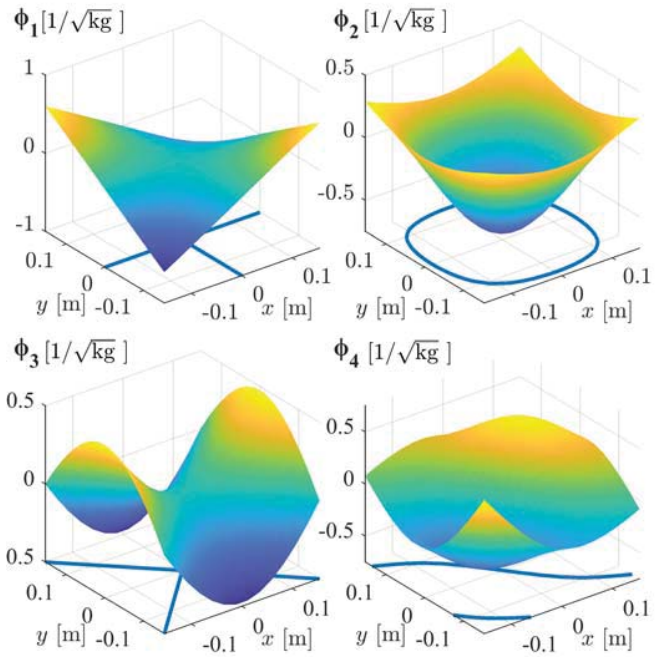

Fig. 4: First four modeshapes of the DLPM translator.

TABLE III: Mass and inertia of the DLPM translator.

Parameter	Variable	Value
mass [kg]	m_{trans}	10.1
inertia around x-axis [kg/m^2]	$I_{x,\text{trans}}$	0.125
inertia around y-axis [kg/m^2]	$I_{y,\text{trans}}$	0.125
inertia around z-axis [kg/m^2]	$I_{z,\text{trans}}$	0.248

The differential equations in (10) can be transformed to a state-space representation

$$\begin{aligned}\begin{pmatrix}\dot{\boldsymbol{\eta}}\\ \ddot{\boldsymbol{\eta}}\end{pmatrix} &= \begin{pmatrix}\mathbf{0} & \mathbf{I}\\ -\boldsymbol{\Omega}^2 & -2\mathbf{Z}\boldsymbol{\Omega}\end{pmatrix}\begin{pmatrix}\boldsymbol{\eta}\\ \dot{\boldsymbol{\eta}}\end{pmatrix} + \begin{pmatrix}\mathbf{0}\\ \boldsymbol{\Phi}_{\text{in}}^{\top}\end{pmatrix}\mathbf{f}_{\text{mag}}\\ \mathbf{q} &= \begin{pmatrix}\boldsymbol{\Phi}_{\text{out}} & \mathbf{0}\end{pmatrix}\begin{pmatrix}\boldsymbol{\eta}\\ \dot{\boldsymbol{\eta}}\end{pmatrix},\end{aligned} \tag{11}$$

where the matrices $\boldsymbol{\Phi}_{\text{in}}$ and $\boldsymbol{\Phi}_{\text{out}}$ represent a selection of the modeshapes that correspond to actuation and measurement locations, respectively. Since 281 permanent magnets are glued to the aluminum plate of the translator, it is assumed that the force on each of the individual magnets produced by a coil, exerts a force on this plate. The force working on a magnet is applied on a node in the top side center of a magnet, where it connects to the aluminum plate. The influence of torque of the individual magnets on the translator deformation is less than 10 % and, therefore, neglected in the input vector [5]. The input vector for (11) is then given by

$$\mathbf{f}_{\text{mag}} = \begin{pmatrix} F_{x_{\text{mag},1}} & F_{y_{\text{mag},1}} & F_{z_{\text{mag},1}} & F_{x_{\text{mag},2}} & \dots & F_{z_{\text{mag},281}} \end{pmatrix}^{\top} \tag{12}$$

where $F_{x_{\text{mag},1}}$ is the force on magnet number 1 in the x-direction, while the dimension of the vector $\mathbf{f}_{\text{mag}}$ is $3 \cdot 281 \times 1$. The mass and inertia coefficients of the magnetic plate are given in Table III.

2) Coil current to modal force relation: The modal force F_{η_n} of mode n is the product of the transpose of the eigenvector and the input forces

$$F_{\eta_n} = \boldsymbol{\phi}_n^{\top}\, \mathbf{f}_{\text{mag}}, \tag{13}$$

and transforms the force on the individual magnets to a force that acts on a specific modeshape. By applying the force on each of the magnets, calculated by the Lorentz force principle for 1 A in a coil, in (13) gives the coupling factor between this coil and the modal force, $k_{F_{\eta_n}}$.

The relation from coil current to modal force is included in the direct wrench-current decoupling algorithm, to decouple the flexible modes from the rigid body modes when actuating the planar motor. In this way, the active coils can be used for overactuation of the system and, hence, to control the flexible modes. The number of active coils has to be larger or equal to the controlled degrees of freedom, which is equal to the rigid body modes plus the number of controlled flexible modes, to allow for an under-determined solution as in (4). For each flexible mode that should be decoupled, an additional row is added to the commutation matrix of (2). The commutation matrix for overactuation is given by

$$\boldsymbol{\Gamma}_{\text{overac}} = \begin{pmatrix} {}^1k_{F_x}(\mathbf{p}) & {}^2k_{F_x}(\mathbf{p}) & \cdots & {}^{N_c}k_{F_x}(\mathbf{p}) \\ {}^1k_{F_y}(\mathbf{p}) & {}^2k_{F_y}(\mathbf{p}) & \cdots & {}^{N_c}k_{F_y}(\mathbf{p}) \\ {}^1k_{F_z}(\mathbf{p}) & {}^2k_{F_z}(\mathbf{p}) & \cdots & {}^{N_c}k_{F_z}(\mathbf{p}) \\ {}^1k_{T_x}(\mathbf{p}) & {}^2k_{T_x}(\mathbf{p}) & \cdots & {}^{N_c}k_{T_x}(\mathbf{p}) \\ {}^1k_{T_y}(\mathbf{p}) & {}^2k_{T_y}(\mathbf{p}) & \cdots & {}^{N_c}k_{T_y}(\mathbf{p}) \\ {}^1k_{T_z}(\mathbf{p}) & {}^2k_{T_z}(\mathbf{p}) & \cdots & {}^{N_c}k_{T_z}(\mathbf{p}) \\ {}^1k_{F_{\eta_n}}(\mathbf{p}) & {}^2k_{F_{\eta_n}}(\mathbf{p}) & \cdots & {}^{N_c}k_{F_{\eta_n}}(\mathbf{p}) \end{pmatrix}, \tag{14}$$

where the bottom row of the matrix decouples flexible mode η_n. For each row that is added in the commutation matrix $\boldsymbol{\Gamma}_{\text{overac}}$, a corresponding wrench entry has to be created

$$\begin{aligned}&\mathbf{w}_{\text{overac}}(\mathbf{p}) = \\ &\begin{pmatrix} F_x(\mathbf{p}) & F_y(\mathbf{p}) & F_z(\mathbf{p}) & T_x(\mathbf{p}) & T_y(\mathbf{p}) & T_z(\mathbf{p}) & F_{\eta_n}(\mathbf{p}) \end{pmatrix}^{\top}.\end{aligned} \tag{15}$$

If the modeshape displacement of a flexible mode is set to zero in the wrench, the coil currents should (ideally) not actuate that particular modeshape. The currents for the overactuation of the system for a given wrench $\mathbf{w}_{\text{overac}}$ and commutation matrix $\boldsymbol{\Gamma}_{\text{overac}}$ are again calculated through (5).

IV. Experimental analysis of coil current to modal displacement relation

To measure the relation from coil current to deformation of the moving-magnet plate as a function of position, a coil is excluded from the commutation, which is used to act as a disturbance on the translator during standstill levitation for a range of positions. The magnetic field to stably levitate the translator is produced by the other 39 active coils. A sinusoidal current is applied in the coil that is excluded from the commutation. By applying a sinusoidal disturbance to the translator at the frequency of a flexible mode, the magnet plate will dominantly resonate at this particular frequency and deform due to the corresponding modeshape. The deformation

of a certain modeshape is reconstructed from deformation amplitudes obtained from frequency analysis of the measurement data. Because the disturbance is applied outside the controller bandwidth (16 Hz), the response of the controller on position fluctuations, resulting from the rigid body position reconstruction of the deforming translator, will be minimal.

The relation from coil current to deformation of the translator is experimentally analyzed as the relation from coil current to modal force that is described in the previous section cannot directly be measured in the DLPM, since the modal force is not a measurable quantity. As a function of the x- and y-position between a coil and the translator, the modal displacement amplitude will show the same relation as the modal force, only with different magnitude which can be computed based on the frequency and damping of the flexible mode. The modal displacement amplitude that is produced when a sinusoidal current is applied in the coil excluded from the commutation, can be calculated from the modal force amplitude as described in [19]. The solution of the modal displacement for mode n as a function of time is given by $\eta_n = \hat{\eta}_n \cos(\omega_F t - \phi_n)$, where ω_F is the frequency of the applied force and ϕ_n the phase shift with respect to the sinusoidal disturbance current. The steady-state deformation amplitude, $\hat{\eta}_n$, is then given by

$$\hat{\eta}_n = \frac{F_{\eta_n}}{\sqrt{\left(\omega_n^2 - \omega_F^2\right)^2 + \left(2\zeta_n \omega_n \omega_F\right)^2}}. \tag{16}$$

When the applied force has the same frequency, or the frequency is close to one of the natural frequencies of the system, which is the case in the experiment, (16) reduces to

$$\hat{\eta}_n \approx \frac{F_{\eta_n}}{2\zeta_n \omega_n \omega_F} \approx \frac{F_{\eta_n}}{2\zeta_n \omega_n^2}. \tag{17}$$

Hence, the modal displacement is, for a sinusoidal input to the system, highly dependable on the damping coefficients of the modes. Since the damping coefficients of the flexible modes of a mechanical structure are difficult to determine, the measurement data and model data are, before comparison, normalized with respect to the rms value of the data on the considered grid.

The relation between a coil current and the flexible mode deformation is highly position dependent, as for various positions between the coil and the translator, a different force is exerted on each of the individual magnets by the coil and, hence, a different modal displacement is produced. The relation from coil current to modal displacement amplitude for a top layer coil is depicted in Fig. 5 for the first four modeshapes. This is the displacement amplitude expected from the model with a disturbance current of 0.3 A and the eigenfrequencies and damping coefficients as given in Table II. The relations in Fig. 5 show that, for example, a coil underneath the center of the translator, where it produces a force in the z-direction, has a high coupling to flexible mode 2, and a negligible coupling to flexible mode number 1. On the other hand, a coil underneath a corner of the translator will have the opposite effect, hence, a high coupling to flexible mode 1 and low coupling to flexible mode 2.

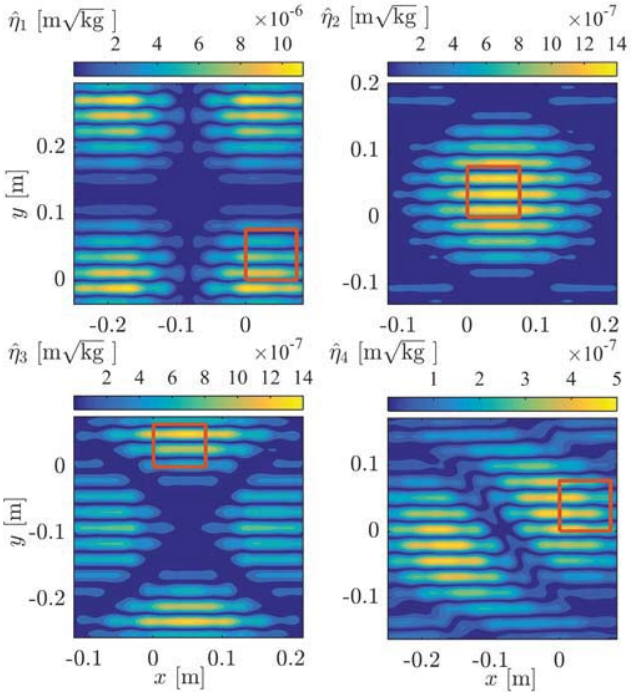

Fig. 5: Coil current to modal displacement amplitude relations for the first four flexible modes. The analyzed area of the position dependent relation for each of the modes is indicated with the red box.

For each flexible mode, a different coil is chosen to excite the translator in order to measure the deformation of this particular mode. In this way, a region where the coupling between the coil current and modal displacement is relatively high, is selected. The measured area for each of the first four flexible modes is indicated in Fig. 5. The translator is moved in the highlighted area on a grid with spacing of 2.0 mm x 2.0 mm. At each position in the grid, the translator is levitated and the sinusoidal current with an amplitude of 0.3 A and frequency of one of the first four flexible modes is applied in the disturbance coil. When the system has reached a steady-state, the position read by each of the 25 interferometers is recorded for 5 seconds ($50 \cdot 10^3$ samples).

To obtain the modal displacement of the flexible mode under consideration, the data of each of the 25 interferometers is processed using the fast Fourier transform (FFT). The average of time domain data is first subtracted from the data itself and is then multiplied with a Hamming window [22], after which the FFT is applied. The amplitudes that are found at a certain position from the FFT of each of the 25 interferometers at the eigenfrequency n under consideration are collected in the column vector $\hat{\mathbf{z}}_{\Delta,n}$. The modal displacement amplitude $\hat{\eta}_n$ is reconstructed using the corresponding column from the output matrix

$$\hat{\eta}_n(x,y) = |\boldsymbol{\Phi}_{\text{out,n}}|^{-1}(x,y)\ \hat{\mathbf{z}}_{\Delta,n}(x,y). \tag{18}$$

The vector $\boldsymbol{\Phi}^{-1}_{\text{out,n}}(x,y)$ is a mapping from the z-displacement seen by the 25 lasers ($\hat{\mathbf{z}}_{\Delta,n}$) to the modal displacement of mode n, for a certain x-, y-position. This vector is obtained

TABLE IV: Error between the measured and modeled coil current to modal displacement amplitude. Both data sets are normalized to their respective rms value over the measurement range before comparison.

	Flexible mode number n			
	1	2	3	4
relative rms error [%]	19.6	14.2	7.8	14.6
maximum relative error [%]	52.3	65.1	20.8	46.1

by interpolation of the output matrix based on the position of the laser interferometer with respect to the center of the translator. The absolute value of this vector is used to obtain the modal displacement amplitude, as the measured deformation amplitudes are also positively valued.

A. Results

The obtained difference between model and measurement is shown in Fig. 6. For the reasons discussed before, the displacement amplitude data as function of position, is normalized with respect to the rms value over the considered area for both the measurement and model before comparison. The relative rms error between the model and measurement over the measured range is obtained by calculating the rms value of the normalized difference shown in Fig. 6 and given in Table IV. The discrepancy between the model and the measurement is position dependent showing different patterns for the four analyzed modes. For all first four modes, the relative rms error over the measured area is less than 20 %, although locally larger errors are observed. The maximum relative error is obtained for flexible mode number 2, where the local discrepancy is approximately 65 %. The errors are originating from discrepancies between the realized translator structure and the mechanical FEM model. The structure of the permanent magnet array and its connection to the aluminum plate is rather complex to mechanically analyze, and this model should, therefore, be further optimized for the DLPM system.

V. Active Compensation of Deformation

Using the commutation as presented in Section III, the deformation of the translator due to the spatial distribution of the force over the plate surface is minimized. To experimentally demonstrate this procedure, a comparison is performed between simulation and experimental data when the translator is levitated and its center is at the position $\mathbf{p} = (203\ \text{mm}\ 203\ \text{mm}\ 203\text{mm}\ 0\ \text{rad}\ 0\ \text{rad}\ 0\ \text{rad})^\top$. First, by using the commutation in (2), where only the rigid body modes are considered, the supplied currents will result in modal force that acts on the translator. By employing (14) including the first four flexible modes and setting their corresponding wrench entries in $\mathbf{w}_{\text{overac}}$ to zero, ideally, the coils produce the required force and torque to levitate the translator while avoiding the excitation of the flexible modes. The reduction of the deformation, $\mathbf{z}_\Delta$, is obtained by

$$\mathbf{z}_\Delta = \mathbf{z}_\Gamma - \mathbf{z}_{\Gamma_{\text{overac}}}, \tag{19}$$

where $\mathbf{z}$ is the displacement data of the 25 LIFM, which is acquired by averaging the time domain data, recorded for 30 seconds. Hence, the difference in deformation is determined between measurements performed with only the rigid body mode commutation and measurements performed with the commutation for overactuation activated.

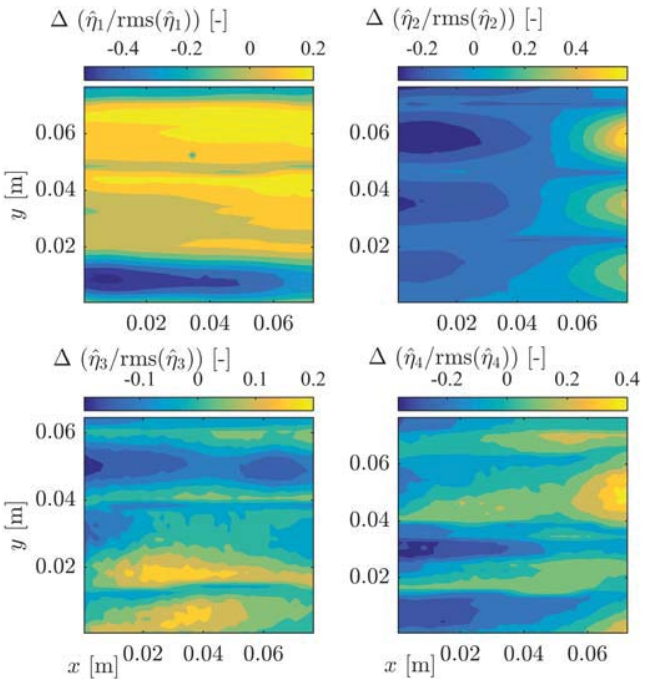

Fig. 6: Difference between the model and measurement for the relation from coil current to model displacement amplitude. The modeled values, normalized to the rms value over the measured range are subtracted from the measured values, normalized to the measured rms value. Top left: Flexible mode 1. Top right: Flexible mode 2. Bottom left: Flexible mode 3. Bottom right: Flexible mode 4.

The position reconstruction from the 9-axis interferometer system is based on the assumption that the system behaves as a rigid body. Therefore, the effect of the deformation will be interpreted as rotation and displacement of the rigid body. Then, to compensate for this effect a straight plane is fitted through the displacement data and removed from this data. The resulting deformation difference is shown in Fig. 7 in blue. The maximum measured deformation reduction is equal to $5.44{\cdot}10^{-7}$ m. The largest part of the deformation is caused by flexible mode 2, which is expected as the coils underneath the center of the translator carry the highest currents for levitation, while they also have the largest coupling with the second modeshape.

To make a comparison with the reduction of the deformation predicted by the model, the modal force exerted by the coils, when only rigid body modes are considered in the commutation, are computed. Using (13) and the supplied currents in this case, the estimated modal forces for the considered position are equal to $F_{\eta_1} = 0.05\ \text{N}/\sqrt{\text{kg}}$, $F_{\eta_2} = -19.17\ \text{N}/\sqrt{\text{kg}}$, $F_{\eta_3} = -2.84\ \text{N}/\sqrt{\text{kg}}$ and $F_{\eta_4} = -1.89\ \text{N}/\sqrt{\text{kg}}$ for the first four flexible modes. By employing (11), the resulting deformation is estimated and shown in Fig. 7 in red. Hence, the displacement data when overactuation is applied in the

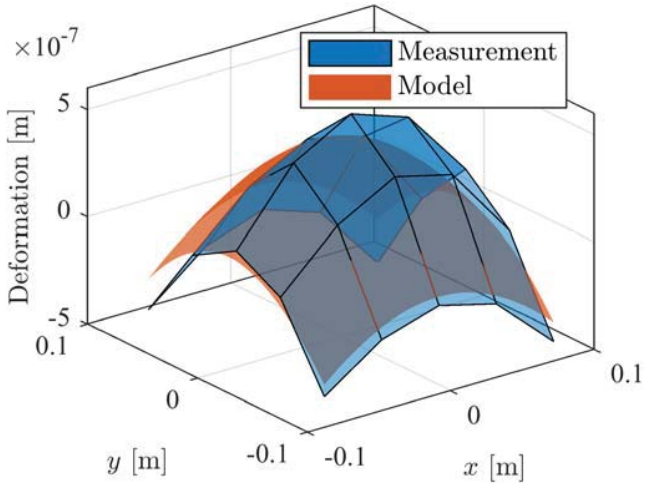

Fig. 7: Deformation reduction when overactuation is activated in the commutation. The blue surface shows the difference in the displacement data measured in the non-overactuated and overactuated case. The red surface shows the predicted deformation reduction.

commutation is not subtracted for the (ideal) model, as no deformation is produced by the coils in this case. The rms error between the predicted response and the measurement is equal to $1.01{\cdot}10^{-7}$ m, which is relative to the maximum measured displacement an error of 18.6 %. With this experiment, the capabilities of the planar motor towards overactuation are demonstrated.

VI. Conclusions

In this paper, the overactuation possibilities of the DLPM are exploited. To this end, a mechanical model for the translator of the planar motor has been developed in a mechanical FEM software and it is coupled to the electromagnetic model. Using the coupled model the relation from coil current to the deformation of a certain flexible mode is computed, resulting in the decoupling of the flexible modes from the rigid body modes and thus allowing for the control of the flexible modes.

The relation from coil current to modal displacement, which is position dependent and obtained from the model, has been compared to experimental data for the first four flexible modes. The maximum relative rms error is found for flexible mode 1, where the relative error was equal to 19.6 %. For the other modeshapes, the relative rms error is smaller than 15 %. This error can be reduced by optimization of the mechanical model of the DLPM.

Using the developed commutation method the compensation of the static deformation of the translator during levitation is enabled. It has been experimentally observed that a deformation reduction by $5.44{\cdot}10^{-7}$ m can be achieved during standstill levitation at a specific position. As a result, the use of the proposed commutation method for the active control of the flexible behavior of the DLPM is experimentally demonstrated.

References

[1] J. M. M. Rovers, J. W. Jansen, and E. A. Lomonova, "Design and measurements of the double layer planar motor," in *Electric Machines Drives Conference (IEMDC), 2013 IEEE International*, May 2013, pp. 204–211.

[2] J. W. Jansen, C. M. M. van Lierop, E. A. Lomonova, and A. J. A. Vandenput, "Magnetically levitated planar actuator with moving magnets," in *2007 IEEE International Electric Machines Drives Conference*, vol. 1, May 2007, pp. 272–278.

[3] Y. Wang, X. Chen, X. Luo, and L. Zeng, "Analysis and optimization of a novel 2-D magnet array with gaps and staggers for a moving-magnet planar motor," *Sensors*, vol. 18, no. 1, 2018.

[4] J. C. Compter, "Electro-dynamic planar motor," *Precision Engineering*, vol. 28, no. 2, pp. 171 – 180, 2004.

[5] J. M. M. Rovers, "Multiphysical modeling of high-precision electromechanical devices : towards nanometer-accurate planar motors," Ph.D. dissertation, Department of Electrical Engineering, 2013.

[6] T. A. E. Oomen, E. Grassens, and F. B. J. W. M. Hendriks, "Inferential motion control : identification and robust control for positioning an unmeasurable point of interest," *IEEE Transactions on Control Systems Technology*, vol. 23, no. 4, pp. 1602–1610, 2015.

[7] R. Voorhoeve, R. de Rozario, W. H. T. M. Aangenent, and T. Oomen, "Identifying position-dependent mechanical systems: A modal approach with applications to wafer stage control," *CoRR*, vol. abs/1807.06942, 2018.

[8] T. Oomen, R. van Herpen, S. Quist, M. van de Wal, O. Bosgra, and M. Steinbuch, "Connecting system identification and robust control for next-generation motion control of a wafer stage," *IEEE Transactions on Control Systems Technology*, vol. 22, no. 1, pp. 102–118, 2014.

[9] M. E. Johnson, L. P. Nascimento, M. Kasarda, and C. R. Fuller, "The effect of actuator and sensor placement on the active control of rotor unbalance," *Journal of Vibration and Acoustics*, vol. 125, no. 3, pp. 365–373, 2003.

[10] V. Tamisier, S. Font, M. Lacour, F. Carrère, and D. Dumur, "Attenuation of vibrations due to unbalance of an active magnetic bearings milling electro-spindle," *CIRP Annals*, vol. 50, no. 1, pp. 255 – 258, 2001.

[11] M. Schneiders, M. Molengraft, van de, and M. Steinbuch, "Modal framework for closed-loop analysis of over-actuated motion systems," in *Proceedings of the 2004 ASME International Mechanical Engineering Congres*, 2004.

[12] J. M. M. Rovers, J. W. Jansen, J. C. Compter, and E. A. Lomonova, "Analysis method of the dynamic force and torque distribution in the magnet array of a commutated magnetically levitated planar actuator," *IEEE Transactions on Industrial Electronics*, vol. 59, no. 5, pp. 2157–2166, May 2012.

[13] J. M. M. Rovers, J. Achterberg, M. J. C. Ronde, J. W. Jansen, J. C. Compter, E. A. Lomonova, C. M. M. van Lierop, and M. J. G. van den Molengraft, "The deformation of the moving magnet plate of a commutated magnetically levitated planar actuator," *Mechatronics*, vol. 23, no. 2, pp. 233 – 239, 2013.

[14] C. M. M. van Lierop, J. W. Jansen, E. A. Lomonova, A. A. H. Damen, P. P. J. van den Bosch, and A. J. A. Vandenput, "Commutation of a magnetically levitated planar actuator with moving-magnets," *IEEJ Transactions on Industry Applications*, vol. 128, no. 12, pp. 1333–1338, 2008.

[15] C. M. M. van Lierop, "Magnetically levitated planar actuator with moving magnets," Ph.D. dissertation, Eindhoven University of Technology, 2008.

[16] G. Golub and C. V. Loan, *Matrix Computations, Fourth Edition*. The Johns Hopkins University Press, 2013.

[17] J. W. Jansen, J. P. C. Smeets, T. T. Overboom, J. M. M. Rovers, and E. A. Lomonova, "Overview of analytical models for the design of linear and planar motors," *IEEE Transactions on Magnetics*, vol. 50, no. 11, pp. 1–7, Nov 2014.

[18] W. Gawronski, *Advanced Structural Dynamics and Active Control of Structures*. Springer New York, 2004.

[19] A. K. Chopra, *Dynamics of Structures: Theory and Applications to Earthquake Engineering*. Pearson/Prentice Hall, 2007.

[20] S. S. Rao and F. F. Yap, *Mechanical vibrations*. Addison-Wesley New York, 1995, vol. 4.

[21] *ANSYS Academic Research Mechanical, Release 17.1*, ANSYS Inc.

[22] A. V. Oppenheim, R. W. Schafer, and J. R. Buck, *Discrete-time Signal Processing (2Nd Ed.)*. Upper Saddle River, NJ, USA: Prentice-Hall, Inc., 1999.